ROTATING MACHINERY
Transport Phenomena

Proceedings of the Third International Symposium on Transport Phenomena and Dynamics of Rotating Machinery (ISROMAC-3)

Edited by

J. H. Kim
Electric Power Research Institute
Palo Alto, California

W.-J. Yang
University of Michigan
Ann Arbor, Michigan

HEMISPHERE PUBLISHING CORPORATION
A member of the Taylor & Francis Group
Washington Philadelphia London

Mean Temperature Measurements of Jets with a Crossflow for Gas Turbine Film Cooling Application

K. A. THOLE, A. K. SINHA, D. G. BOGARD, and M. E. CRAWFORD
Mechanical Engineering Department
University of Texas
Austin, Texas 78712, USA

ABSTRACT

This paper presents mean temperature profiles measured within and downstream of a row of inclined jets with a crossflow. The conditions for the experiments are representative of film cooling used on gas turbine blades. A range of density ratio between 1.2 and 2.0 was examined under different mass, velocity, and momentum flux ratios of the jet to mainstream. Of these film cooling parameters, the momentum flux ratio best scaled the characteristics of the thermal field. The film cooling jets were found to remain attached to the surface; to detach and then reattach to the surface; or to detach and remain detached from the surface. These three scenarios and also the vertical jet penetration distance into the mainstream were found to scale with the momentum flux ratio. These results which establish the point at which detachment occurs have obvious relevance to turbine blade film cooling. The velocity ratio and mass flux ratios were found to be inadequate scaling parameters for the thermal fields.

NOMENCLATURE

D	injection hole diameter
DR	density ratio, jet to mainstream, $DR = \rho_j/\rho_\infty$
I	momentum flux ratio, jet-to-freestream, $I = \rho_j U_j^2/\rho_\infty U_\infty^2$
k	thermal conductivity
M	mass flux ratio or blowing rate, jet to freestream, $M = \rho_j U_j/\rho_\infty U_\infty$
$Re_{\delta 2}$	Reynolds number based on momentum thickness, $Re_{\delta 2} = U_\infty \delta_2/\nu$
T	mean temperature
T_{aw}	adiabatic surface temperature
T_j	temperature of the injected fluid
T_∞	freestream temperature
U_j	average jet velocity at the exit of the hole
U_∞	freestream velocity
VR	velocity ratio, average jet velocity to mainstream, $VR = U_j/U_\infty$
X	downstream distance from the leading edge of the hole
Y	vertical distance measured from the test surface
Z	lateral distance measured from the axis of the hole
α	coefficient of thermal expansion
ρ	density
θ	non-dimensional temperature, $\theta = (T - T_\infty)/(T_j - T_\infty)$
η	adiabatic wall effectiveness $\eta = (T_{aw} - T_\infty)/(T_j - T_\infty)$
δ_1	boundary layer displacement thickness

δ_{99}	boundary layer thickness
δ_2	boundary layer momentum thickness
ν	kinematic viscosity

INTRODUCTION

Because designers are increasing the entry temperatures to turbines to improve propulsion efficiencies, new cooling schemes for the turbine blade are required to prolong the blade's life. Film cooling is a turbine cooling technique in which the blade surface is protected from high temperature mainstream gases by releasing a coolant through the surface. In the blade (or vane) cooling process, the compressor bleed air is introduced into the hollow core of the blade and is channeled and then dumped through the blade surface via one or more rows of holes. The holes are typically located in the vicinity of the leading edge of the blade and at other high thermally loaded locations on the blade's suction and pressure surfaces. The heat transfer process is an external convection/conduction/internal convection process in which the resulting external and internal heat fluxes set the blade temperature. The coolant is intended to help reduce the external heat flux to the blade.

Cooling jets emerging at various locations along the surface interact with the boundary layer flow along the surface and the hot mainstream. Governing the flow field of the jet-mainstream interaction and the associated heat transfer are geometrical parameters such as hole shape, angle, and spacing; and fluid dynamic parameters such as coolant-to-mainstream ratios of density (DR), velocity (VR), blowing or mass flux (M), and momentum flux (I). Most previous research has focused on how these parameters influence the wall temperature for an adiabatic wall. These results are generally presented in terms of a normalized wall temperature which is known as the adiabatic wall effectiveness, η. Relatively few studies have investigated the thermal and flow fields associated with the film cooling.

The adiabatic wall effectiveness is primarily dependent on how the cooling jet interacts with the mainstream. The thermal field is important because it directly shows the jet-mainstream interaction. For example, Ramsey and Goldstein (1971) used temperature profiles, measured at a sequence of four streamwise locations, to track the "penetration of the jet" at two different blowing ratios. In a later study, Yoshida and Goldstein (1984) used temperature profile measurements to distinguish differences in jet trajectories and mixing with the mainstream when the jet and mainstream conditions changed from laminar to turbulent.

Several studies have been conducted in which a heavy molecular weight gas is used to obtain higher density for the cooling jets. The technique relies on the use of the heat-mass transfer analogy to relate the measured species concentration field to the thermal field. This analogy holds if the turbulent and molecular Lewis numbers are unity, as noted by Ito et. al. (1978). Similar to the thermal profile measurements, concentration profile measurements have been used to determine the penetration of the cooling jets into the mainstream. In particular, Foster and Lampard (1980) used measurements of concentration profiles at a sequence of four streamwise locations to establish "jet lift-off." They noted that this jet lift-off was not clearly evident from mean velocity profiles measured at the same streamwise locations. Ko et. al. (1982) also established jet lift-off using a concentration profile measured a short distance downstream of the hole.

The importance of the thermal field is indicated by the computational study of Demuren et. al. (1985) in which discrepancies between computed and measured cooling effectiveness were resolved by referring to computed and measured temperature fields. Differences between predicted and measured cooling effectivenesses were found to be due to distinct differences in the computed and measured temperature fields in the near wall region, although the overall

temperature fields were qualitatively the same.

Although thermal or concentration field measurements are clearly superior for determining the trajectory of the cooling jets, previous studies have not established the effect of parameter variations. In particular, the thermal field with respect to mass flux, velocity, or momentum flux ratios has not been evident in previous studies because of the limited range of parameter variations – one or two blowing ratios at a constant density ratio.

Since the density ratio is generally about DR = 2 for gas turbine film cooling, the effect of high density ratios is important. Moreover, varying the density ratio over a wide range is the only way to independently vary the key flow parameters M, VR, and I. The only previous work in which systematic variations of density ratio were used to determine appropriate scaling parameters for film cooling were studies by Pederson, Eckert, and Goldstein (1977) and Sinha, Bogard, and Crawford (1990). Using a foreign gas injectant, Pederson et al. varied the density ratio from 0.2 to 4 with a range of blowing ratios and measured the effects on η. Along the centerline at a position X/D = 10 downstream of the hole, they found that the maximum η always occurred at approximately VR = 0.5 with increasing η at higher density ratios. For VR > 0.8, η at different density ratios scaled with velocity ratio, but for VR < 0.4, η was found to scale with momentum flux ratio. Sinha et. al. (1990) used thermal techniques to determine adiabatic effectiveness for density ratios ranging from 1.2 to 2.0. Their results showed that the centerline effectiveness scaled with mass flux ratio while the jet remained attached to the wall, but scaled best with momentum flux ratio when the jet began to detach.

Pietrzyk, Bogard, and Crawford (1989b) presented detailed velocity data for density ratios of DR = 1 and DR = 2 with a range of blowing ratios. In the near hole region the velocity ratio was found to be a good parameter for scaling density effects. In the far-field region, the velocity fields for the dense jets were similar to that for the unit density case with the same mass flux ratio. The high density jets had significantly lower relaxation rates for the turbulence levels and $\overline{uv}$ shear stresses as compared with the low density jets.

In this study, measurements of the thermal field were made to complement previous measurements of the velocity field of Pietrzyk et. al. (1989a and 1989b). The thermal field shows certain characteristics that the velocity field cannot show. The thermal field measurements also give a better indication of the jet trajectory and jet lift-off as compared to velocity field measurements. The thermal field measurements combined with previous velocity field measurements provide an important database for developing and verifying film cooling models. The experimental conditions for this study were achieved by cryogenically cooling the injectant to vary the density ratio while independently varying the mass flux, the momentum flux, and the velocity ratios. A major goal of this study was to determine how each of these parameters scaled the entire thermal field as the density ratio varied. Previously reported studies of the thermal field (concentration field) have not been extensive enough to show variation in the jet trajectory and diffusion as M, VR, and I are varied.

FACILITY AND INSTRUMENTATION

Experiments were performed using a closed loop wind tunnel with a secondary flow loop that provided cryogenically cooled air for controlling the jet density, as depicted in Fig. 1. A flat test plate was used with a single row of inclined holes. A brief description of the facility is given here; but further details can be found in Pietrzyk, Bogard, and Crawford (1989a and 1989b).

Figure 2 shows the geometry of the film-cooled test plate and the coordinate system. The

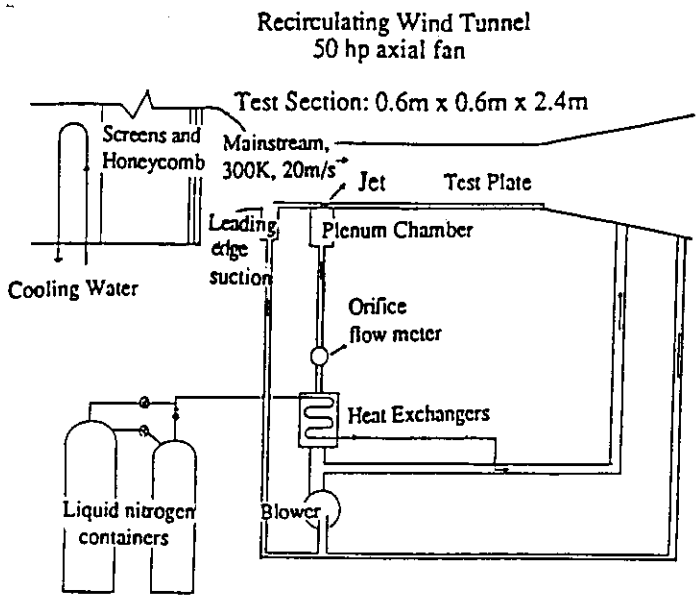

FIGURE 1. Schematic of the the film cooling test facility.

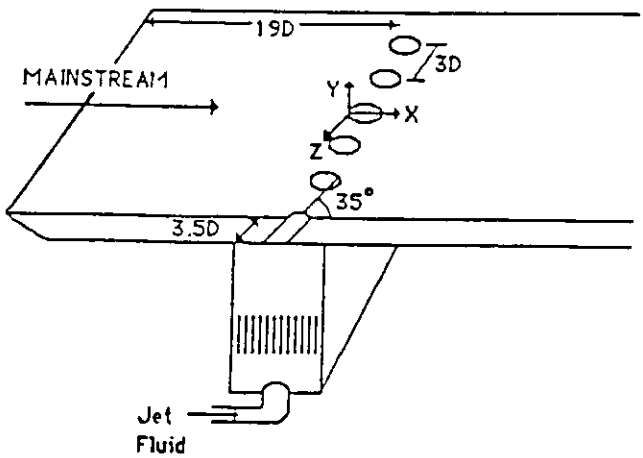

FIGURE 2. Film cooling test geometry and coordinate system.

cryogenically cooled air was injected through a row of 11 holes, 12.7 mm in diameter and spaced 3 diameters apart in the spanwise direction. The holes, having a length-to-diameter ratio of 3.5, were inclined at 35 degrees and located 19 diameters downstream of the leading edge of the test plate. The test plate and plenum chamber were constructed from a glass

reinforced plastic material (commercially known as EXTREN) with low thermal expansion coefficient ($\alpha = 1.4 \times 10^{-5}$ per K) and relatively low thermal conductivity (k = 0.58 W/m/K). Surface roughness measurements verified that the plate was hydrodynamically smooth.

Initial Boundary Layer Conditions

A 50 hp axial fan located in the closed loop recirculating wind tunnel provided the mainstream flow. Suction was used to remove the boundary layer upstream of the test section, and a new boundary layer was initiated at the sharp leading edge of the test plate that formed the test section floor. The suction rate was set based on measurements of the pressure differential across the leading edge of the plate. Laser Doppler velocimetry measurements showed that this ensured parallel flow above the leading edge. A heat exchanger, located between the blower and the wind tunnel contraction, maintained the freestream temperature at 298 K ± 0.5 K. For all experiments the freestream velocity was 20 m/s ± 1 % and the freestream turbulence intensity was 0.2 %. The freestream velocity was uniform within ± 0.5 % in both the spanwise and streamwise directions. The streamwise development of the turbulent boundary layer on the test plate was documented by Pietrzyk et. al. (1989a), who showed that at the injection location (X/D = 0), the non-dimensional boundary layer thickness δ_{99}/D was $\delta_{99}/D = 0.58$, the non-dimensional boundary layer displacement thickness was $\delta_1/D = 0.10$, and the momentum-thickness Reynolds number was about $Re_{\delta_2} = 1090$.

A thin, uniform thermal boundary layer in the spanwise direction was formed due to the cold plenum chamber which extended from X/D = -5 to X/D = 3 below the test plate. The maximum normalized temperature, measured in the thermal boundary layer between holes at X/D = 3 and at Y/D = 0.08 above the wall, was less than $\theta = 0.05$, which was below the lowest temperature contour appearing on our plots. The approaching thermal boundary layer is insignificant when compared to the thermal boundary layer formed by the film cooling jets and thus not expected to alter the temperature field.

Conduction errors in the test plate were estimated using a three-dimensional conduction heat transfer code. Based on these calculations, the normalized surface temperatureds were expected to be reduced by as much as $\Delta\eta = 0.3$ near the hole, and by $\Delta\eta = 0.1$ at X/D = 10. Despite these relatively large surface conduction errors, measurements showed that air temperatures were relatively unaffected as low as Y/D = 0.01.

Secondary Flow Loop

Cryogenically cooling the air in a secondary flow loop provided the injectant at a controllable density ratio. A 7.5 hp blower directed the air in the secondary flow loop through a set of four finned-tube heat exchangers arranged in series. Liquid nitrogen, supplied by a pressurized 160 liter dewar, was used as the coolant in the heat exchangers. The jet temperature was maintained within ± 1.5 K of the required operating temperature.

The mass flowrate of the fluid in the secondary flow loop was measured using a sharp-edged orifice plate flow meter. To obtain accurate flowrate measurements, the air temperature was measured at the orifice meter. Temperatures in the secondary flow loop and the plenum supplying the jets of coolant were measured using chromel-constantan thermocouples. Accuracy of the thermocouples was verified using four set points provided by boiling distilled water (373.2 K), ice (273.2 K), dry ice (194.4 K), and liquid nitrogen (77.4 K).

The temperatures recorded by the readout instrument were within 0.1 K, which was the resolution of the instrument. Maximum temperature fluctuations at the orifice meter were ± 2.5 K, and the measurement of total mass flowrate of the jets was accurate within ± 0.7 %. Due to the accumulation of the frost in the secondary flow loop, the mass flowrate varied by as much as ± 4 % during experiments. The density ratio between the jets and the mainstream was maintained within ± 3%. To check the variation in flowrate from different jets, the mean velocity was measured at five vertical positions at two streamwise locations for five different jets in the center of the test section. These measurements showed the variation of flowrate among the jets to be within ± 4%. The temperature variation among the jets varied by less than ± 1K.

Temperature Measurement Instrumentation

Air and wall temperatures were measured during the experiments. A TSI model 1050 hot-wire anemometer was operated in a constant current mode to obtain cold-wire measurements of the mean air temperature. A 4 micron diameter, tungsten wire with a sensor length of 0.76 mm was used. The cold-wire was calibrated in the mainstream and at the exit of the cooled jets where the air temperature was measured using thermocouples. The voltage/temperature correlation remained linear within 1.5% which was verified at jet temperatures of 247 K, 186 K, 166 K, and 150 K. The precision of traversing the temperature sensor was ± 0.01 mm normal to the wall and ± 0.5 mm in the streamwise direction. Taking into account the position uncertainty, the total uncertainty of the non-dimensional air temperatures (θ to be defined later) was ± 0.035.

Chromel-constantan thermocouples measured the wall temperatures. Initial testing of an EXTREN plate showed that large conduction errors resulted from installing the lead wires to the thermocouples through the EXTREN plate. The primary source of the conduction errors was the large driving potential between the ambient and the cold surface, resulting in equilibrium temperatures of the bead that were significantly higher than that of the surface.

To eliminate the conduction error, ribbon contact surface thermocouples were developed. Sinha et. al. (1990) report the details of the surface temperature measuring technique. The ribbon thermocouples were nominally conduction-error free because of the large convective surface area relative to its small conduction cross-sectional area. The chromel and constantan ribbons were 1.5 mil thick and 60 mil wide with a junction diameter of approximately 15 mil. The thermocouples were joined by spot welding negative (constantan) ribbons to a single positive (chromel) ribbon. An epoxy bonded the thermocouples to the EXTREN plate. The non-dimensional surface temperatures were measured to within an accuracy of ± 0.006.

EXPERIMENTAL PLAN

Since a constant mass flux ratio would maintain a constant energy flux ratio, one might expect the thermal field to scale with M as the density ratio changes. However, as discussed in the Introduction, Pietrzyk et. al. (1989b) found that the velocity field in the near hole region scaled with velocity ratio. With equal velocity ratios, the velocity gradients and the volumetric flowrates at different density ratios are similar. Pietrzyk et. al. (1989b) also noted that there appeared to be greater penetration for the higher density jet which had greater momentum flux ratio. Since the deflection of the jets leaving the hole depends on the momentum flux ratio, the momentum flux ratio should dictate the jet trajectory. Therefore, the thermal field, which is strongly dependent on the velocity field will be influenced by all three parameters, M, VR, and I. Consequently a series of experiments were designed to

systematically investigate the scaling of the thermal field with respect to M, VR, and I.

A list of the experimental conditions and the corresponding case and figure numbers of the data represented by temperature contours are presented in Table 1. Note that Cases 2, 3 and 4 were at constant velocity ratio, Cases 4, 7, and 8 were at constant mass flux ratio, and Cases 4, 5, and 6 were at constant momentum flux ratio.

TABLE 1. Range of Experimental Parameters

Case	Momentum Flux Ratio	Density Ratio	Velocity Ratio	Mass Flux Ratio	Figure Number
1	0.125	2.0	0.25	0.5	5
2	0.35	1.4	0.5	0.7	8
3	0.4	1.6	0.5	0.8	9
4	0.5	2.0	0.5	1.0	6
5	0.5	1.2	0.65	0.78	10
6	0.5	1.6	0.56	0.89	11
7	0.63	1.6	0.63	1.0	12
8	0.83	1.2	0.83	1.0	13
9	2.0	2.0	2.0	2.0	7

Mean temperature profiles were taken along the jet centerline (Z/D = 0) at a number of streamwise stations extending from the leading edge of the jet (X/D = 0) to 10 diameters downstream. The trailing edge of the hole extends to a streamwise location of X/D = 1.74. The gradients in the thermal field were effectively resolved by concentrating data points in regions of high gradients. The number of points in a profile varied depending on the streamwise location. Most of the figures presented in this paper to document the thermal fields are in form of contours, the levels of which were obtained by linearly interpolating between the data points. The data have been non-dimensionalized using the freestream and jet temperatures, and are presented in terms of a non-dimensional parameter, θ, defined by equation (1) as

$$\theta = \frac{T - T_\infty}{T_j - T_\infty} \qquad (1)$$

RESULTS AND DISCUSSION

Whether or not a film cooling jet remains attached to the surface after it exits the hole is relevant to the protection the jet can give the turbine blade surface. If the jet remains attached, the coldest temperatures will occur at the blade surface to give the best possible protection. However, if the jet detaches from the surface immediately downstream of the hole, warmer temperatures occurring downstream of the jet exit would be detrimental to the blade.

Figure 3 shows the non-dimensional temperature profiles at three different streamwise locations for the lowest momentum flux ratio (I = 0.125) jet studied in these experiments. These profiles show the maximum θ occurs at the surface which indicates that at all three locations the film cooling jet remained attached to the surface. Also shown in Figure 3 are surface temperatures measured at X/D = 6 and 10. The zero temperature gradients immediately above the wall show that the plate is essentially adiabatic in terms of heat flux into the air. However, there is a significant difference between the air temperature immediately above the plate and the surface temperature. This difference is due to conduction effects within the plate which were discussed in the Facilities and Instrumentation section.

Figure 4 shows non-dimensional temperature profiles at three streamwise locations for the full range of density ratios (DR = 1.2, 1.6, and 2) at the same intermediate momentum flux ratio (I = 0.5). Even though these profiles were measured at significantly different density ratios, the profiles collapse to similar shapes. At this intermediate momentum flux ratio, the X/D = 2 profiles show steep gradients of θ at the surface. The steep gradients above the wall at X/D = 2 indicate either a conduction effect from the plate or a slightly detached jet with an influx of warm air under the jet. The thermal contours discussed below show that the shape of the profile at X/D = 2 can be attributed to detachment of the jet with an influx of warm under the jet, and not due to a conduction effect from the plate. At X/D = 6, it is difficult to determine whether the jet has reattached to the surface or is still detached, while at X/D = 10 the non-dimensional temperature profiles are similar to those of an attached jet.

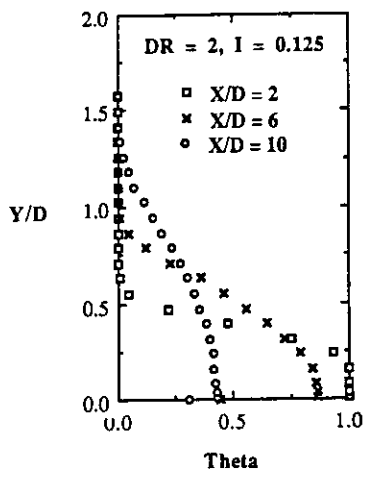

FIGURE 3. Dimensionless temperature profiles at three streamwise locations, X/D = 2, X/D = 6, and X/D = 10, for I = 0.125, DR = 2, VR = 0.25, M = 0.5.

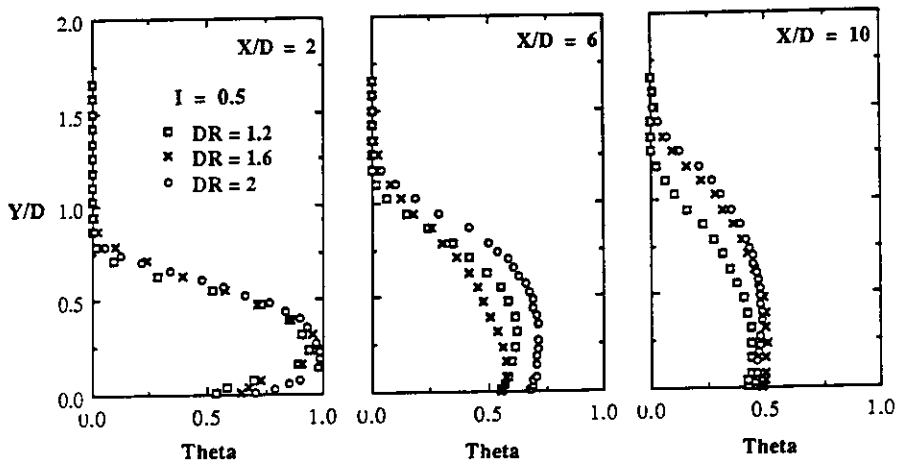

FIGURE 4. Dimensionless temperature profiles at three streamwise locations, X/D = 2, X/D = 6, and X/D = 10 for a constant momentum flux ratio (I = 0.5).

To determine whether the jet remains attached or detaches, contours of the complete thermal field were analyzed . Figures 5, 6, and 7 show the thermal fields for a series of experiments in which the density ratio was held constant at DR = 2.0 and the momentum flux ratio was varied such that the jet remains attached, detaches and then reattaches, and detaches and stays detached, respectively. Note that the θ contours in Figures 5 and 6 are for the same conditions as the θ profiles shown in Figures 3 and 4, respectively.

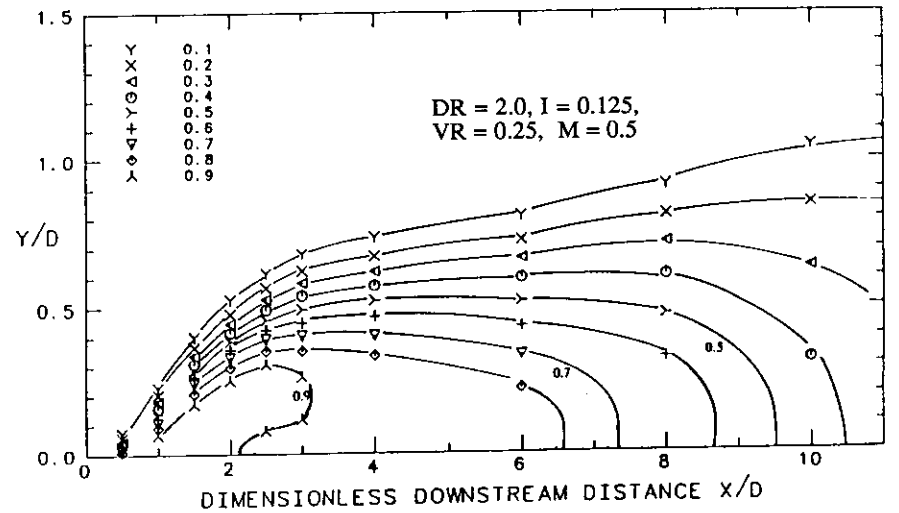

FIGURE 5. Dimensionless temperature contours along the jet centerline for I = 0.125, DR = 2.0, VR = 0.25, M = 0.5.

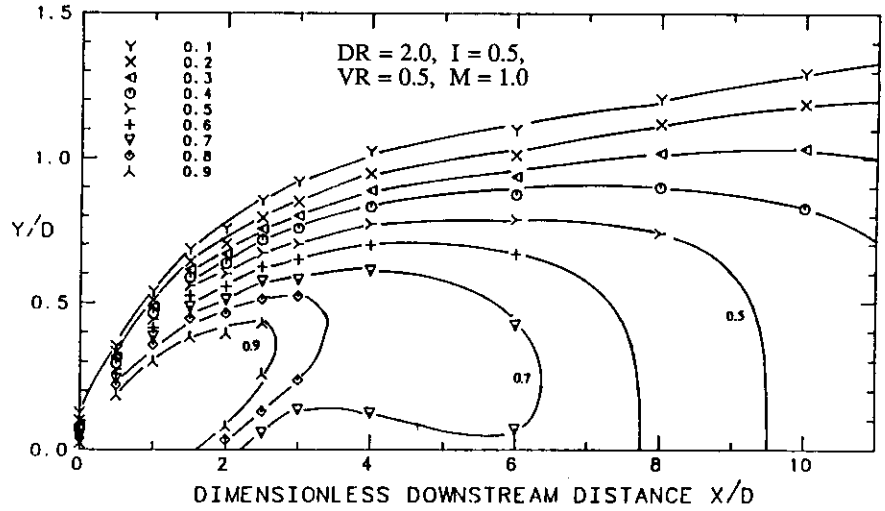

FIGURE 6. Dimensionless temperature contours along the jet centerline for I = 0.5, DR = 2.0, VR = 0.50, M = 1.0.

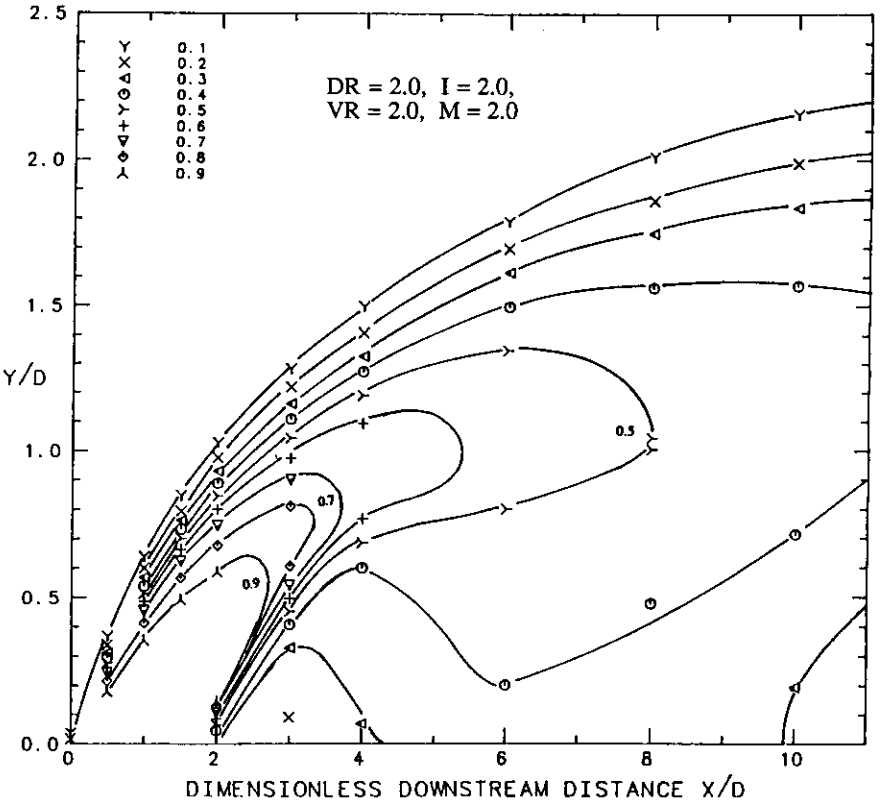

FIGURE 7. Dimensionless temperature contours along the jet centerline for I = 2.0, DR = 2.0, VR = 1.0, M = 2.0.

At low momentum flux ratios the jet remains attached to the surface as indicated by the contours shown in Figure 5 for a jet with I = 0.125. All of the contour levels less than $\theta = 0.9$ are perpendicular to the surface with the peak level (coldest temperature) at any given X/D position occurring at the wall. In contrast, Figure 6 shows an example of a higher momentum flux jet (I = 0.5) which has detached and then reattached to the surface. The $\theta = 0.7$ contour level in Figure 6 has been pushed over by the mainstream consequently being deflected toward the surface. The "curl" of the $\theta = 0.7$ contour is representative of the jet which initially detaches and then is deflected towards the surface and consequently reattaches to the surface. The contours indicate that the coldest temperature does not occur at the surface until slightly before X/D = 8 where the $\theta = 0.6$ contour level does not fold back on itself, and is instead perpendicular to the surface. For a jet with a still higher momentum flux ratio, I = 2, the contours shown in Figure 7 clearly indicate that the jet remains detached from the surface. Note that the contour levels from $\theta = 0.9$ to 0.5 close back on themselves and the maximum θ occurs much above the surface indicating a large warm air region under the jet. Given that the center of the jet is represented by the maximum θ level at each streamwise position, the jet appears to level out a little above Y/D = 1 and does not come back towards the surface.

Penetration of the jet into the mainstream also varies with momentum flux ratio. Because the low momentum jet shown in Figure 5 is flattened onto the surface and remains attached to the surface, the vertical penetration distance of the $\theta = 0.1$ contour of the jet at X/D = 10 is only slightly greater than Y/D = 1. Figure 6 shows that for an intermediate momentum flux ratio the jet has penetrated the mainstream to a height of Y/D = 1.3 by X/D = 10. Finally, Figure 7 shows the detached jet to have the largest penetration distance of Y/D = 2.2 at X/D = 10.

Although changes in jet conditions described above were attributed to changes in momentum flux ratio, scaling of the thermal field with respect to the velocity ratio or mass flux ratio has not been addressed. In the following sections we will show that the detachment–reattachment characteristics of the jets scale with the momentum flux ratio and not the velocity ratio, nor the mass flux ratio.

Momentum Flux Ratio Scaling

Three distinct ranges of momentum flux ratios were identified from the analysis of the non-dimensional temperature contours. The three ranges will be referred to as the low momentum flux ratio range ($I < 0.4$), the intermediate momentum flux ratio range ($0.4 < I < 0.8$), and the high momentum flux ratio range ($I > 0.8$). A discussion of each of the momentum flux ratio ranges follows.

In the low I range, the low momentum jets are flattened on to the plate causing the jets to remain attached to the surface as seen by the temperature contours shown in Figures 5, and 8. The momentum flux ratios for Figures 5 and 8 are I = 0.125 and 0.35, respectively. The thermal field shown in Figure 5 shows that all of the temperature contours greater than 0.9 come into the surface perpendicular indicating the jet is attached to the surface. However, Figure 8, which has a slightly greater momentum flux ratio, shows that between the exit of the hole (X/D = 1.74) and X/D = 3.5, the 0.8 contour level is not perpendicular to the surface. Thus, the coldest temperature does not occur at the surface indicating a slight separation region very near the exit of the hole. This low range of momentum flux ratio is of special relevance for film cooling applications because the surface is getting the most "effective" cooling by the jet at the particular streamwise location.

For momentum flux ratios in the intermediate range $0.4 < I < 0.8$, the thermal fields in both

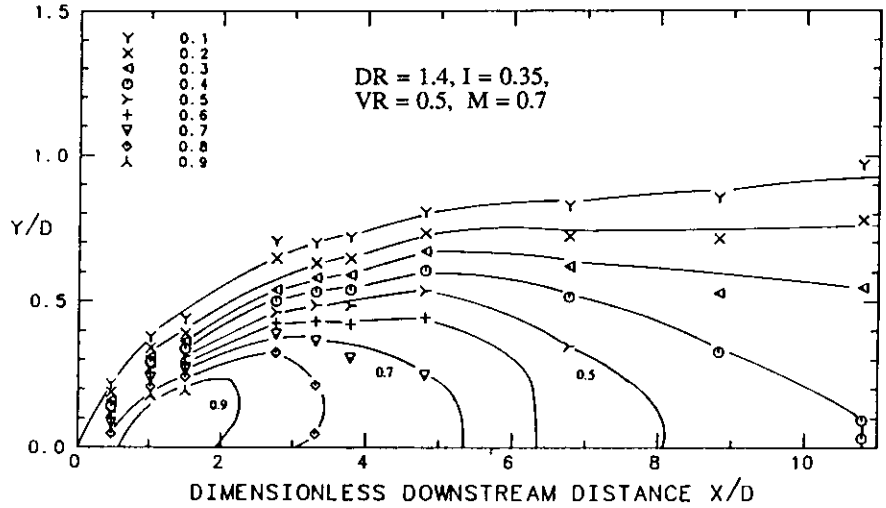

FIGURE 8. Dimensionless temperature contours along the jet centerline for I = 0.35, DR = 1.4, VR = 0.5, M = 0.7.

the near and the far fields appear quite similar which is indicated by the contours shown in Figures 9, 6, 10, 11, and 12 (stated in order of increasing momentum flux ratio). In the thermal field for a momentum flux ratio of I = 0.4, shown in Figure 9, the $\theta = 0.7$ contour is curling back toward the surface indicating jet reattachment, similar to that previously shown in Figure 6. Further downstream the $\theta = 0.5$ and 0.6 contour levels in Figure 9 are perpendicular to the surface indicating a reattached jet.

The non-dimensional temperature contours for a constant momentum flux ratio (I = 0.5) are

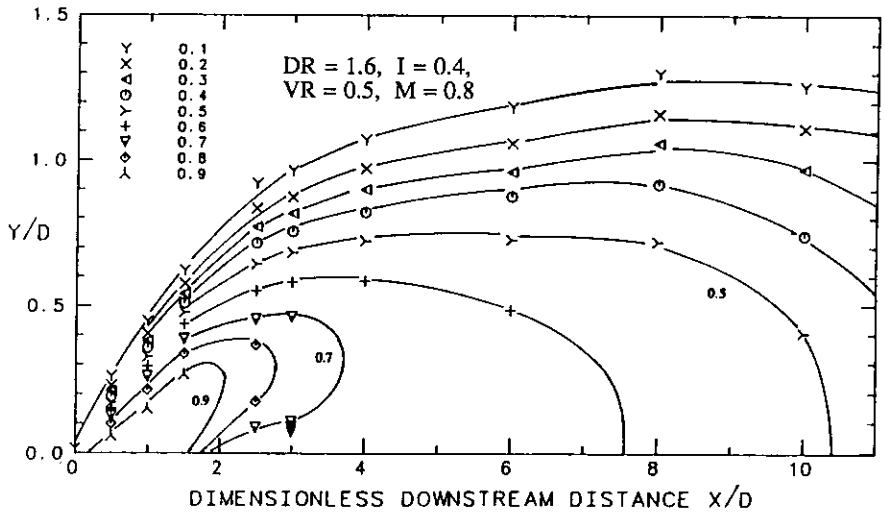

FIGURE 9. Dimensionless temperature contours along the jet centerline for I = 0.40, DR = 1.6, VR = 0.5, M = 0.8.

shown in Figures 6, 10 and 11. As stated previously, the corresponding profiles for I = 0.5, shown in Figure 4, collapse quite well for the full density ratio range studied in these experiments. All three of the jets at this intermediate momentum flux ratio (I = 0.5) show the curl over of the contour levels downstream of the film cooling hole, which is characteristic of the detaching/reattaching jet. The θ = 0.7 contour level in Figures 6, 10, and 11 best exhibits this curling over. Figures 10 and 11 show a θ = 0.6 contour "bubble" appearing because of the warm air nestled below the separated jet. The appearance of this bubble, representing higher temperatures (lower θ contours) below the jet also occurs in

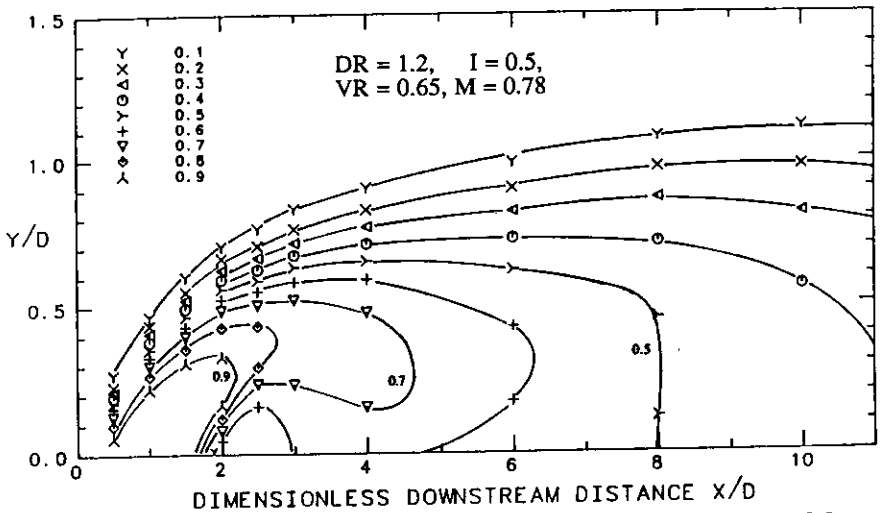

FIGURE 10. Dimensionless temperature contours along the jet centerline for I = 0.5, DR = 1.2, VR = 0.65, M = 0.775.

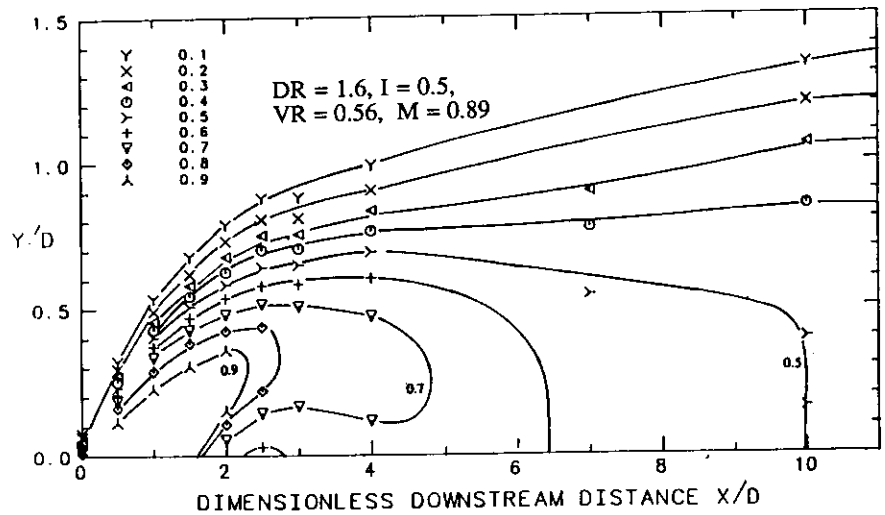

FIGURE 11. Dimensionless temperature contours along the jet centerline for I = 0.5, DR = 1.6, VR = 0.56, M = 0.89.

Figure 12 which shows the thermal field for a slightly greater momentum flux ratio (I = 0.63). This warm air bubble is also characteristic of a jet which has detached and then reattached. The warmer temperatures existing in this bubble next to the surface are detrimental to surface cooling, and hence the streamwise length of this warm region is significant.

In the high I range, the jet has enough momentum as it leaves the hole to penetrate far into the mainstream and remain detached from the surface as seen in Figures 13 and 7 (stated in

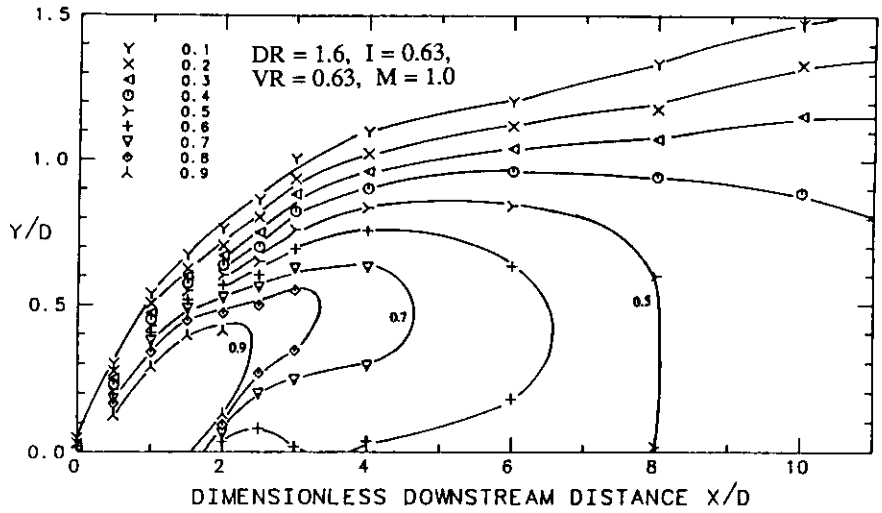

FIGURE 12. Dimensionless temperature contours along the jet centerline for I = 0.63, DR = 1.6, VR = 0.63, M = 1.0.

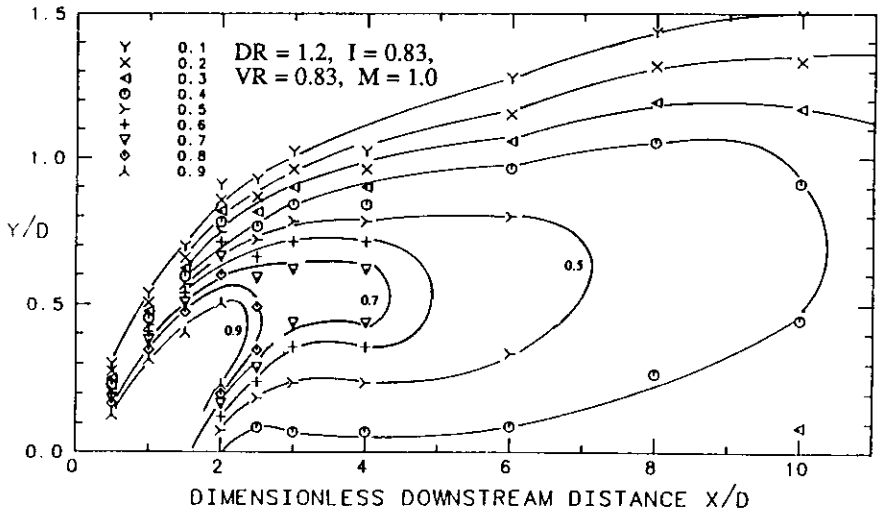

FIGURE 13. Dimensionless temperature contours along the jet centerline for I = 0.83, DR = 1.2, VR = 0.83, M = 1.0.

increasing I). Figure 13 shows that peak temperatures are displaced away from the wall. Immediately above the wall the θ levels are less than θ = 0.4 and as a consequence the "effectiveness" of the film cooling has degraded.

Temperatures for a fully detached jet can be compared to temperatures for a jet which remains attached to the surface by looking at the θ = 0.5 contours in Figures 5 and 7 for the lowest and highest momentum flux ratio jets, respectively. Even though in both cases the θ = 0.5 temperature contour is sustained close to the same downstream location (X/D = 9.5 for the attached jet and X/D = 8 for the detached jet), the θ = 0.5 level for the detached jet occurs much above the surface, thereby not protecting the surface. Although, the fully detached jet spreads towards the surface, the jet is not very useful in helping protect the surface because it is diluted by the mainstream air before reaching the surface.

Velocity Ratio Scaling

The scaling of the overall thermal field with momentum flux ratio is far better than that with velocity ratio. The velocity ratio parameter might appear to be a good scaling parameter when comparing the characteristics of the thermal fields presented in Figures 10 and 12 which have nearly the same velocity ratios (0.65 and 0.625, respectively). However, the velocity ratio parameter clearly fails to scale the thermal fields presented in Figures 6, 8, and 9 which also have a constant velocity ratio (VR = 0.5).

Scaling of the thermal field immediately above the hole exit was also examined in terms of momentum flux ratio and velocity ratio. Pietrzyk (1989) showed that the velocity field at the hole exit scaled with the velocity ratio. Pietrzyk deduced that a separation region occurred at the entrance to the hole which caused the jet to skew towards the upstream side hole at a high velocity ratio and towards the downstream side at a low velocity ratio. Thus, it is reasonable to expect the thermal field just above the exit of the hole to also scale with velocity ratio. However, when comparing the θ profiles above the film cooling hole (at X/D = 1.5) for constant velocity ratio, Figure 14, and constant momentum flux ratio, Figure 15, better

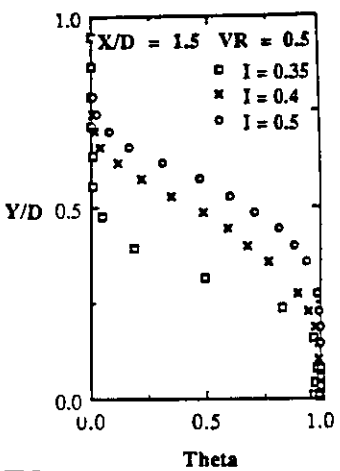

FIGURE 14. Dimensionless temperature profiles at a streamwise location of X/D = 1.5 for a constant velocity ratio (VR = 0.5).

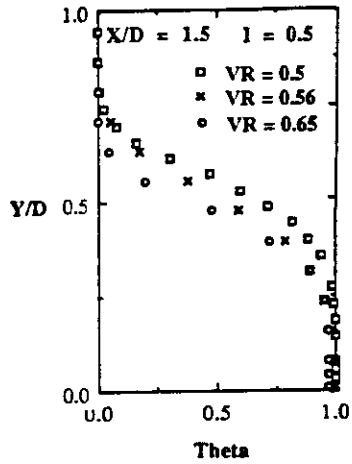

FIGURE 15. Dimensionless temperature profiles at a streamwise location of X/D = 1.5 for a constant momentum flux ratio (I = 0.5).

scaling is found for the momentum flux ratio. There is a relatively good collapse of the temperature profiles for a range of density ratios from DR = 1.2 to 2.0 at constant momentum flux, but there is approximately a 50% variation in the thickness of the profiles for constant velocity ratio. Evidently the thermal field above the hole is more strongly influenced by the deflection of the jet which depends on the momentum flux ratio, even though the velocity field at the jet exit scales with velocity ratio.

Mass Flux Ratio

The mass flux ratio was also investigated as a scaling parameter for the thermal field. Figures 6, 12, and 13 give the θ contours at a constant mass flux ratio (M = 1) for the full range of density ratios. Figures 9 and 10 also give θ contours for approximately the same mass flux ratio ($M \approx 0.8$). It is apparent that the mass flux ratio does not scale the detachment/reattachment scenarios. At the same mass flux ratio the thermal fields in Figures 6 and 12 show a detaching/reattaching jet while Figure 13 shows a detached jet. Similarly, the jet in Figure 9 is not as severly detached as the jet shown in Figure 10. Although the vertical penetration depths are similar for the $M \approx 0.8$ cases as seen in Figures 9 and 10, the vertical penetration depths are significantly different when comparing Figure 6 to Figures 12 and 13 for the M = 1 cases. Thus, the penetration depth does not scale with mass flux ratio.

Relevance to Previous Research

This phenomenon of the jet detaching and then reattaching to the surface was deduced in the past by Ko et. al. (1982), who observed a peak in the adiabatic wall effectiveness downstream of the hole. However, in the absence of a wide parameter range, they attributed the reattachment distance of the jet to changes in the mass-flux ratio. The measurements conducted in this study establish that the reattachment distance is a function of the momentum-flux ratio.

Detachment and reattachment of the film cooling jet was also deduced by Sinha et. al. (1990) based on adiabatic effectiveness measurements. The results of Sinha et. al. were in agreement with the present results in that the detachment and reattachment of the jet scaled with momentum flux ratio.

SUMMARY AND CONCLUSIONS

A detailed study of the thermal fields at different density, mass, velocity, and momentum flux ratios was carried out. The thermal fields were analyzed in terms of non-dimensional temperature profiles and contours. The governing characteristics of the thermal field were identified by whether the film cooling jet remained attached to the surface; detached and then reattached to the surface; or remained fully detached from the surface.

The momentum flux ratio was proven to be the scaling parameter which dictated the attached/detached state of the jet. The following three distinct ranges of the momentum flux ratio were identified: $I < 0.4$ where the jet remains attached to the surface; $0.4 < I < 0.8$ where the jet detaches and then reattaches to the surface; and $I > 0.8$ where the jet remains detached from the surface. Penetration of the jet into the mainstream was also found to scale with the momentum flux ratio.

The mass flux ratio and velocity ratio parameters were inadequate in scaling the thermal characteristics of the film cooling jets investigated.

ACKNOWLEDGEMENT

The authors gratefully acknowledge Wright-Patterson Research and Development Center and the Garrett Engine Division of the Allied-Signal Aerospace Company for support of this research. We also appreciate the assistance from David Dotson, Keith Matocha, and Kenneth Leonore.

REFERENCES

Demuren, A.O., Rodi, W., Schonung, B., 1985, "Systematic Study of Film Cooling with a Three-Dimensional Calculation Procedure," 1985 Beijing International Gas Turbine Symposium and Exposition, ASME Paper 85-IGT-2.

Foster, N.W., and Lampard, D., 1978, "The Flow and Film Cooling Effectiveness Following Injection Through a Row of Holes," Journal of Engr. for Power, Vol. 100, p. 303.

Ko, S-Y, Liu, D-Y, Yao, Y-Q, Li J., and Tsou, F.K., 1982, "Film Cooling Effectiveness of Discrete Holes Measured by Mass Transfer and Laser Interferometer," Seventh Annual International Heat Transfer Conference.

Pederson, D.R., Eckert, E.R.G., and Goldstein, R.J., 1977, "Film Cooling with Large Density Differences between the Mainstream and Secondary Fluid Measured by the Heat-Mass Transfer Analogy," ASME Journal of Heat Transfer, Vol. 99, pp. 620-627.

Pietrzyk, J.R., 1989, "Experimental Study of the Interaction of Dense Jets with a Crossflow for Gas Turbine Applications," Ph.D. Dissertation, University of Texas at Austin.

Pietrzyk, J.R., Bogard, D.G., and Crawford, M.E., 1989a, "Hydrodynamic Measurements of Jets in Crossflow for Gas Turbine Film Cooling Applications", Journal of Turbomachinery, Vol. 111 pp. 139-145.

Pietrzyk, J.R., Bogard, D.G., and Crawford, M.E., 1989b, "Effects of Density Ratio on the Hydrodynamics of Film Cooling, " ASME Paper No. 88-GT-194.

Ramsey, J.W., and Goldstein, R.J., 1971, "Interaction of A Heated Jet with a Deflecting Stream," ASME Journal of Heat Transfer, Vol. 93, p. 365.

Sinha, A.K., Bogard, D.G., and Crawford, M.E., 1989, "Film Cooling Effectiveness Downstream of a Single Row of Holes with Variable Density Ratio," Submitted for presentation at the International Gas Turbine Conference, Brussels, Belgium.

Yosida, T., and Goldstein, R.J., 1984, " On the Nature of Jets Issuing From a Row of Holes into a Low Reynolds Number Mainstream Flow," Journal of Engineering for Gas Turbines and Power, Vol. 106, p. 612.